Chapter 2
Characterization of Geographical and Meteorological Parameters

G. Montero, E. Rodríguez and A. Oliver

Abstract This chapter is devoted to the introduction of some geographical and meteorological information involved in the numerical modeling of wind fields and solar radiation. Firstly, a brief description of the topographical data given by a Digital Elevation Model and Land Cover databases are provided. In particular, the Information System of Land Cover of Spain (SIOSE) is considered. The study is focused in the roughness length and the displacement height parameters that appear in the logarithmic wind profile, as well as in the albedo related to solar radiation computation. An extended literature review and characterization of both parameters are reported. Next, the concept of atmospheric stability is introduced from the Monin-Obukhov similarity theory to the recent revision of Zilitinkevich of the Neutral and Stable Boundary Layers (SBL). The latter considers the effect of the free-flow static stability and baroclinicity on the turbulent transport of momentum and of the Convective Boundary Layers (CBL), more precisely, the scalars in the boundary layer, as well as the model of turbulent entrainment.

2.1 Geographical data

The main geographical information for wind and solar radiation modeling may be classified into two general databases, the topographical data related to the orography of the region to be studied and the land cover databases containing the information of the land uses. In this section, both are introduced.

Gustavo Montero · Eduardo Rodríguez · Albert Oliver
University Institute for Intelligent Systems and Numerical Applications in Engineering, University of Las Palmas de Gran Canaria, Edificio Central del Parque Tecnológico, Campus de Tafira, 35017, Las Palmas de Gran Canaria, Spain e-mail: gustavo.montero@ulpgc.es, eduardo.rodriguez@ulpgc.es, albert.oliver@ulpgc.es

2.1.1 Topographical information

To study the orography of a surface, it is usual to start from a Digital Elevation Model (DEM) that contains elevation data on a uniform grid (height map). For example, the National Geographic Institute of Spain provides a 25m $\times$25m grid with a precision of 5m in height for all the national territory (MDT25). In Spain, the geodetic Cartesian reference frame used is the European Terrestrial Reference System 1989 (ETRS89) in the Peninsula, Balearic Islands, Ceuta and Melilla, and REGCAN95 in the Canary Islands (both systems are compatible with WGS84). UTM projection in the corresponding time zone is also applied, with an extended time zone 30 for sheets of time zones 29 and 31. This DEM was obtained by interpolation from land cover data obtained with LIDAR of the National Plan of Aerial Orthophotography (PNOA), except for the sheets of Ceuta, Melilla and Alborn Island (1110, 1111, 1078B). They were constructed by automatic stereo-correlation of photogrammetric flies (PNOA) with resolution from 25 to 50 cm/pixel, revised and interpolated with break lines where it was viable.

2.1.2 Land cover databases

The characterization of both the aerodynamic roughness length (z_0) and the displacement height (d) is critical when modeling the wind field using the log vertical profile. It is known that the values of these parameters depend on weather conditions and land coverage. Thus, many authors have studied its relationship, providing typical values for each land cover. In this chapter, we have performed a comprehensive literature review to collect the intervals of z_0 and d values for each land coverage [60]. In particular, we have focused on the coverages present in the "Information System of Land Cover of Spain" (SIOSE).

There are many geometrical factors and atmospheric conditions than can influence the aerodynamic parameters of surfaces and, hence, the vertical wind profiles found above (see, e.g. [54] showing the influence of z_0 in wind speed). Therefore, it is essential to know of the roughness length and the displacement height to define the wind state in numerous applications, such as the wind field, air quality and forest fire spread modeling. The values of z_0 and d are generally related to the vegetation and topographical characteristics so that they are affected by the land coverage variations; for example, the change of season (especially in vegetation cover), construction or demolition of buildings, etc. In addition, for each coverage, z_0 and d estimations may vary according to the wind speed and direction, and the atmospheric stability; see, e.g., [7]. Under this assumption, maps of z_0 and d are built for each weather conditions. As a rule of thumb, we can compute their values as a function of the height of the surface morphology characteristics (h). For instance, for a crop or forest canopy [10] proposes a value of d between $0.67\,h$ and $0.75\,h$, and a value of z_0 about $0.12\,h$. However, these approximations cannot be applied if

the surface is not homogeneous. In such cases, a more detailed analysis of the land coverage is required [47, 48].

For this reason, during the last five decades, many authors have proposed parameterizations for several land coverages. In these first approaches, the characteristics of the surface elements were used to estimate the roughness parameters for the various canopies. For example, with regard to crop canopies, [42] estimated z_0 according to h and d for harvested wheat; [93] obtained z_0 and d as a function of h for olives orchards; and [41] parameterized z_0 from wind measures using the wind profile. In forests, [100] estimated z_0 and d according to the tree crown and structure, while [63] obtained them from wind observations and canopy structure. On the other hand, [20] performed a parameterization from measures in a desert with artificial vegetation, whereas [99] did it from wind speed, temperature and turbulent flow measures in bare soils. Moreover, in urban terrains, [30] compared several formulae of these parameters, and [56] carried out a parameterization of z_0 and d in a heterogeneous surface that was validated using a wind tunnel and empirical data. In wetlands, [61] obtained z_0 and d from the minimization of a least square difference function based on the log wind profile equation for near-neutral stability; in wet grasslands and reed-beds, [1] estimated z_0 from eddy correlation measurements; and [78] used specific parameterizations for a Siberian bog. For water surfaces, some approaches were gathered, such as the estimation of z_0 for the sea that was validated in the laboratory by [39]; the comparison of two parameterizations for oceans by [22]; and the parameterization of z_0 for the sea by [25]. Finally, some authors have also parameterized z_0 and d for general land coverage: [92] proposed changes in Raupach parameterization using a list of values from the literature; [29] compared three previous methods and proposed to use the median; and, in the model of the European Wind Atlas [90], a parameterization of z_0 and d was introduced in four classes of coverages.

Some other authors estimated z_0 and d values according to canopy form. For example, [8] used catastral databases, whereas [14] applied a characterization of buildings in urban terrains. In particular, [84] estimated d in Tokyo considering buildings of different heights. Most of these methods require costly field works. However, the methodology proposed here avoids measuring problems related to the evaluation of roughness parameters. In other approaches, the wind profile is directly used to estimate z_0 and d from wind measurements at different heights over a homogeneous surface from within the inertial sublayer. In their work, [52] estimated z_0 and d for cotton, orchards and desert covers from wind measures using the wind profile; [36] obtained z_0 and d from measures of different instruments; [5] calculated z_0 and d from wind measures and wind profile with radar in desert; [73] and [68] used anemometer measures at different heights for cliff coverage; [11] estimated z_0 and d from field measures in peatlands; [83] obtained z_0 and d from friction velocity ($u^\star$) measures using the wind profile; [13] used different measure equipment and compared results with other authors in desert; [67] presented a regression of data obtained with radio-wind probes in forest; [45] obtained d from simultaneous scintillation measurements at two heights. Both parameters can be estimated by solving

the non-linear wind profile equations: see, e.g., [26] for seas and land, and [18] for forest canopy.

Some applications of particular models and their database have been considered in this study. In [82], z_0 and d were estimated with several numerical models and measured data for cotton, scrub and grass canopies; [57] used a computational fluid dynamics (CFD) simulation and the land cover database of the National Land Agency of Japan; [38] performed a simulation with COAMPS W-UCM for several episodes in New York; [44] used the model COSMO to parameterize z_0 in urban terrains; [91] applied the LGN3 database in Rotterdam; [55] compared results of z_0 and d from the National Land Cover Database (NLCD) for the Conterminous United States [24] with field measures in floodplain surfaces; and [97] presented a project for evaluating the annual wind energy production with a CFD code, a digital land model and three land cover databases. Relevant summaries extracted from several sources may be found in [34], where an extended review of many estimations of z_0 and d is provided, and in [28], where a useful list of parameter values is presented.

Special attention is paid to studies involving the use of remote sensing. On the one hand, the use of aircraft Lidar surveys was presented in [31] where z_0 was obtained for roads; in [37], describing a totally automated approach to the generation of z_0 values from Lidar terrain data; in [88], using a combination of low and high density airborne Lidar and satellite SPOT-5 HRG data, in conjunction with ground measurements of forest structure, to parameterize four models for d and z_0 over cool-temperate forests in an inland river basin; and also in [15] for an application in an inland river basin. On the other hand, in the last twenty-five years, several projects on land cover mapping have been developed mainly using satellite images. They characterize both parameters for each surface type. For example, the LGN7 model that uses several databases in The Netherlands with NSD (National Satellite Data) and aerial photos [35]; the LGN3 land cover database of The Netherlands that combines satellite and ancillary data [98]; the NLCD [24]; the CORINE land cover database [6]; and the SIOSE land cover database of Spain [64] that has been used in this work.

In general, most of the previous methods estimate fixed values of z_0 and d of particular land coverages. The final aim of constructing roughness parameter maps is to improve the mesoscale predictions using a downscaling model; allowing to obtain a more accurate estimation of the wind power that may be generated in a region.

2.1.3 SIOSE land cover database

In 1990, the first land cover database encompassing the whole national territory was constructed in Spain on a scale of 1 : 100.000. It was developed in the framework of the CORINE Land Cover (CLC) European project. In the year 2000, there was a need to update the database to homogenize and improve its utility for developing territorial analysis and European policies. The resulting database is known as Im-

age & CORINE Land Cover 2000. This update led to a new land cover database for the entire European continent. Other CLC updates have been produced in 2006 and 2012. In short, it consists of an inventory of land cover in 44 classes. The CLC uses a Minimum Mapping Unit (MMU) of 25 hectares (ha) for areal phenomena and a minimum width of 100 m for linear phenomena. The time series are complemented by change layers, which highlight changes in land cover with an MMU of 5 ha. The CLC is produced by the majority of countries, by visual interpretation of high-resolution satellite imagery. In a few countries, semi-automatic solutions are applied, using national in-situ data, satellite image processing, GIS integration and generalization. In comparison with the NLCD of the United States of America, the CLC has the advantage that it contains vectorized polygon data instead of the raster data of the NLCD. Also, some layers of the CLC, like fruit trees or olive groves, are missing in the NLCD. However, the NLCD brings some better aspects like up-to-date data, a very high resolution of 30 m/pixel and an available companion dataset with canopy density.

The project SIOSE (Spanish acronym for Information System of Land Cover of Spain) was created in 2005 by the National Reference Center on Land Cover and on Land Use and Spatial Planning to integrate the local information available from the Autonomous Communities and the General State Administration. It uses the geodetic Cartesian reference frame ETRS89 with UTM Projection on time zones 28, 29, 30 and 31, and INSPIRE Directive. Since the requirements at the Spanish national level were higher than those supplied by the European project, the SIOSE generated a new land cover database for all the country on a 1 : 25.000 scale. It was based on reference images from 2005, with a MUM of 0.5 to 2 ha (SIOSE 2005) and a planimetric accuracy of 5 m or better. The project was updated in 2009 and 2011; see [64]. Other important differences with the CLC are the land classification and the hierarchy levels, which are much more simplified in the CLC than in the SIOSE.

The SIOSE inventory is based on reference information, satellite SPOT5 imagery, as geometrical and time reference, and orthophotographs of the National Aerial Orthophotography Plan (PNOA). It uses the cadastre; the Integrated Water Information System (SIA); the Geographical Information System of Agricultural Parcel (SIGPAC); the database of boundary lines between Autonomous Communities from the Central Register of Cartography of the National Geographic Institute; orthophotographs and satellite imagery; databases and thematic maps related to the land cover; the Spanish Forest Map (MFE); and the Map of Crops and Utilization (MCA) provided by the Autonomous Communities, previously approved by the Project National Direction.

The SIOSE database consists of different basic and compound coverages. A compound coverage is made up of a combination of basic or compound coverages. Specifically, it considers eight general groups of basic coverages (Crops, Grassland, Forest, Scrubs, No Vegetation, Artificial Coverage, Wet Coverage and Water Coverage) that are further refined into forty specific classes of basic land coverage; see. e.g., [65]. Therefore, at any point of the terrain, the land cover is defined as a weighted average of these forty basic coverages. The spatial unit is the polygon.

Each polygon must contain a basic or compound coverage. The coverages that represent at least 5% of the polygon surface should be considered. In practice, each point of the DEM grid is labeled with the types of SIOSE polygon where it belongs. Figure 4.2 shows the polygons of the land cover classes in Gran Canaria (6,983) and La Palma (2,470).

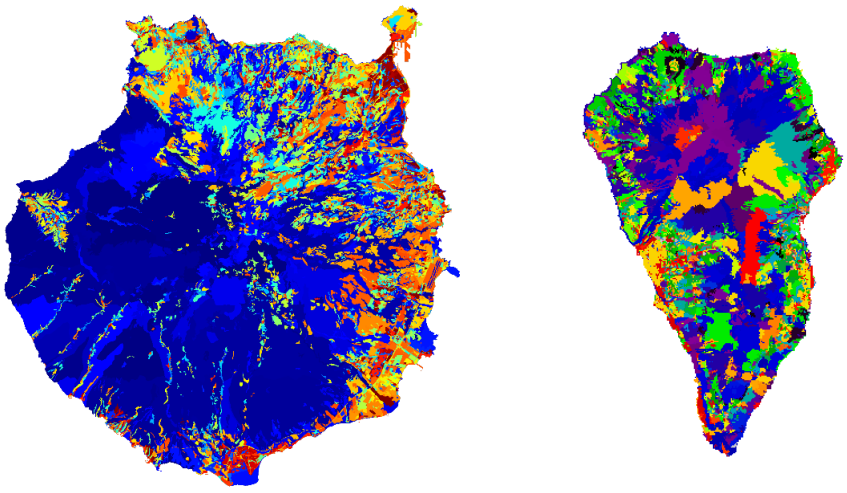

(a) Gran Canaria (b) La Palma

Fig. 2.1: SIOSE land cover polygons for the Islands of Gran Canaria and La Palma, respectively.

2.1.4 Roughness length and displacement height: literature review

The search spaces of z_0 and d must be defined to obtain the appropriate values of them. Here, we present a methodology to generate a table with the ranges of z_0 and d values for each land coverage. Particularly, the methodology is applied to Gran Canaria and La Palma Islands, but it is suitable to any other location. To find the ranges of possible z_0 and d values for each land cover, we have carried out a literature review. Table 2.1 summarizes it and the specific references are listed in the caption. The first and second columns show the SIOSE code and a description for each of the distinct land coverages. The third and fourth, and the fifth and sixth columns present the nominal value and the range of the parameter z_0 and d, respectively. When data are not available, we have used the rule of thumb to obtain the z_0 and d values from

the canopy height h; see [10]. Also, it is worth remarking that d is assumed to be zero for water surfaces (ACU, AEM, AES, ALC, ALG, AMO and LAA classes).

Table 2.1 considers both general and local characteristics of the land coverage. On the one hand, for the most common coverage types in Gran Canaria, we have used the largest interval from those proposed by a wide list of authors. On the other hand, due to the particular characteristics of some land coverages in Gran Canaria, we have used a more specific study in some cases. For instance, the works of [73] and [24] have been employed to characterize sea cliffs. The former study proposes a value of $d = 3.3\,m$ for a cliff of $40\,m$. Using this same ratio, the value for the Andén Verde ($690\,m$) and the Risco de Faneque ($1027\,m$) cliffs are $57\,m$ and $85\,m$, respectively. These values have been taken as lower bound ($3.3\,m$), nominal value ($57\,m$) and upper bound ($85\,m$). Another specific land coverage of Gran Canaria is the LOC class (Other Woody Crops). In Gran Canaria, it refers to Aloe Vera plantations. In this case, [58] studied the typical canopy height ranges for the Aloe Vera. Using these ranges and the rule of thumb, we have obtained the z_0 and d ranges and nominal values.

We have searched in the literature the minimum and the maximum values of each parameter and canopy. In addition, the values more used by different authors have been selected as nominal values, but these are not used in our approach. In fact, we used the ranges of Table 2.1 as searching space for the solution of each parameter in each characteristic wind situations. Then, we performed an extended literature review on the assigned values of the roughness parameters of each coverage. For this reason, in general, we think that the proposed ranges completely cover the variation interval of z_0 and d corresponding to each coverage, respectively, not only for the region studied in this paper but also for any region if the specific coverage is included in that literature review. Nevertheless, some ranges have been defined according to the local characteristics of certain coverages. This is the case of the high sea cliffs in Gran Canaria, for example, where the range of z_0 and d have been adapted to such heights. Another case is Other Woody Crops related to Aloe Vera plantations on the island. For the latter, we have used the standard morphological characteristics. So, in general, these are the only particular cases to review for the application of ranges given in Table 2.1 to any other region.

The bibliography of Table 2.1 may be classified according to the procedure used to obtain z_0 and d. Several authors proposed parameterizations of the roughness parameters from measures of the wind and other physical magnitudes. This is the case of [10] which is used here in many coverages; [90] in water surfaces; [51] in screes; [79] in screes, conifers, and citrus fruit trees; [86, 87] in conifers; [46] in rice crops; [30] in low buildings; [93] in olive groves; [40] in vineyards; [74] in water surfaces; and [32] in artificial coverages.

Some other works are based on the canopy morphology, such as [12] used in water and saline coverages; [53] in deciduous forests, wetlands and scrubs; and [58] in Aloe Vera crops. Another extended approach is the use of measurements and wind profile: [73] used in cliffs; [13] in screes; [5] in Quaternary lava flow; [18, 36, 67] in conifers; [83] in rice crops; [41] in crops different from rice; [70] in no citrus fruit

Table 2.1: Nominal values and ranges of z_0 and d for the land cover classes provided by SIOSE. The superindex indicates the source: (a) [24], (b) [73], (c) [3], (d) [90], (e) [6], (f) [10], (g) [12], (h) [4], (i) [75], (j) [98], (k) [101], (l) [51], (m) [13], (n) [79], (o) [5], (p) [18], (q) [36], (r) [67], (s) [86, 87], (t) [83], (u) [46], (v) [16], (w) [41], (x) [23], (y) [74], (z) [89], (α) [30], (β) [53], (γ) [28], (δ) [21], (ϵ) [17], (ζ) [57], (η) [9], (θ) [43], (ι) [59], (κ) [70], (λ) [58], (μ) [93], (ν) [72], (ξ) [40], (σ) [95], (τ) [26], (ϕ) [32], (χ) [82], (ψ) [81], (ω) [96].

Code	**Land Cover**	z_0 (m)	z_{0min}–z_{0max}	d (m)	d_{min}–d_{max}
ACM	Sea Cliffs	$0.05^{(a)}$	$0.05^{(b)}$–$0.19^{(b)}$	$57^{(b)}$	$3.3^{(b)}$–$85^{(b)}$
ACU	Water Courses	$0.00025^{(c)}$	$0.0001^{(d)}$–$0.01^{(e)}$	$0^{(f,y)}$	–
AEM	Water body. Reservoirs	$0.00025^{(d)}$	$0.0001^{(d)}$–$0.005^{(g)}$	$0^{(f,y)}$	–
AES	Estuaries	$0.0002^{(h)}$	$0.0001^{(d)}$–$0.01^{(e)}$	$0^{(f,y)}$	–
ALC	Coastal Lagoons	$0.005^{(g)}$	$0.0001^{(d)}$–$0.01^{(e)}$	$0^{(f,y)}$	–
ALG	Water body. Lakes and Lagoons	$0.0005^{(i)}$	$0.0001^{(d)}$–$0.005^{(g)}$	$0^{(f,y)}$	–
AMO	Seas and Oceans	$0.0002^{(h)}$	$0.0001^{(d)}$–$0.03^{(a)}$	$0^{(f,y)}$	–
ARR	Rocky Outcrops and Rocks	$0.005^{(e)}$	$0.0003^{(j)}$–$0.18^{(k)}$	$0.03^{(f)}$	$0^{(f)}$–$0.96^{(f)}$
CCH	Screes	$0.1^{(a)}$	$0.05^{(l)}$–$0.15^{(m)}$	$0.6^{(n)}$	$0.56^{(n)}$–$0.66^{(n)}$
CLC	Quaternary lava flow	$0.0286^{(o)}$	$0.0013^{(o)}$–$0.0735^{(o)}$	$0.15^{(f)}$	$0^{(f)}$–$0.4^{(f)}$
CNF	Forest. Conifers	$1.28^{(p)}$	$0.25^{(q)}$–$1.93^{(r)}$	$13.1^{(s)}$	$4.87^{(r)}$–$22^{(n)}$
CHA	Herbaceous crops. Rice	$0.072^{(t)}$	$0.001^{(u)}$–$0.11^{(t)}$	$0.85^{(t)}$	$0.1^{(t)}$–$1.55^{(t)}$
CHL	Herbaceous crops. Different from Rice	$0.1^{(v)}$	$0.004^{(w)}$–$0.74^{(x)}$	$0.25^{(w)}$	$0.1^{(w)}$–$3^{(\iota)}$
EDF	Artificial Coverage. Buildings	$1.5^{(z)}$	$0.7^{(z)}$–$3.7^{(x)}$	$14^{(z)}$	$7^{(z)}$–$19.73^{(f)}$
FDC	Forest. Leafy. Deciduous	$1^{(\beta)}$	$0.18^{(\beta)}$–$1.4^{(a)}$	$11.8^{(\gamma)}$	$3^{(\gamma)}$–$21.6^{(\gamma)}$
FDP	Forest. Leafy. Evergreen	$0.72^{(k)}$	$0.6^{(c)}$–$2.65^{(\delta)}$	$9.7^{(\gamma)}$	$3^{(\gamma)}$–$31^{(z)}$
GNP	No Vegetation. Glaciers and Perpetual Snow	$0.001^{(e)}$	$0.00001^{(\epsilon)}$–$0.012^{(z)}$	$0.01^{(f)}$	$0^{(f)}$–$0.06^{(f)}$
HMA	Salt Marshes	$0.11^{(k)}$	$0.0002^{(j)}$–$0.17^{(j)}$	$0.6^{(f)}$	$0^{(f)}$–$0.93^{(f)}$
HPA	Wetlands	$0.1^{(e)}$	$0.005^{(\beta)}$–$0.55^{(k)}$	$0.55^{(f)}$	$0.03^{(f)}$–$3^{(f)}$
HSA	Salt Mines	$0.01^{(e)}$	$0.0005^{(e)}$–$0.04^{(g)}$	$0.05^{(f)}$	$0^{(f)}$–$0.22^{(f)}$
HSM	Salt Lakes	$0.01^{(e)}$	$0.0005^{(e)}$–$0.04^{(g)}$	$0.05^{(f)}$	$0^{(f)}$–$0.22^{(f)}$

Table 2.1: *Continued*

Code	Land Cover	$z_0\,(m)$	z_{0min}–z_{0max}	$d\,(m)$	d_{min}–d_{max}
HTU	Peat bogs	$0.03^{(e)}$	$0.0005^{(e)}$–$0.03^{(e)}$	$0.16^{(f)}$	$0^{(f)}$–$0.16^{(f)}$
LAA	Artificial Coverage. Artificial water body	$0.0001^{(e)}$	$0.0001^{(e)}$–$0.005^{(g)}$	$0^{(e,y)}$	–
LFC	Woody Crops. Citrus Fruit Trees	$0.31^{(\eta)}$	$0.03^{(d)}$–$0.4^{(\theta)}$	$3^{(n)}$	$0^{(\iota)}$–$4^{(\iota)}$
LFN	Woody Crops. No Citrus Fruit Trees	$0.25^{(e)}$	$0.03^{(d)}$–$1^{(\zeta)}$	$0.92^{(\kappa)}$	$0^{(\iota)}$–$4^{(\iota)}$
LOC	Other Woody Crops	$0.0615^{(\lambda,f)}$	$0.0369^{(\lambda,f)}$–$0.0861^{(\lambda,f)}$	$0.33^{(\lambda,f)}$	$0.2^{(\lambda,f)}$–$0.47^{(\lambda,f)}$
LOL	Olive Groves	$0.48^{(\mu)}$	$0.25^{(e)}$–$0.61^{(\mu)}$	$2.67^{(\mu)}$	$2^{(\mu)}$–$3^{(\mu)}$
LVI	Vineyards	$0.2^{(\nu)}$	$0.08^{(\xi)}$–$0.55^{(\nu)}$	$0.75^{(\nu)}$	$0.31^{(\xi)}$–$1.4^{(\sigma)}$
MTR	Scrubs	$0.16^{(\beta)}$	$0.016^{(\beta)}$–$1^{(a)}$	$4.8^{(\tau)}$	$0.9^{(z)}$–$7.1^{(\tau)}$
OCT	Artificial Coverage. Other Buildings	$0.5^{(e)}$	$0.06^{(k)}$–$1^{(e)}$	$4^{(\alpha)}$	$2^{(\alpha)}$–$14^{(z)}$
PDA	No Vegetation. Beaches, Dunes and Sandy Areas	$0.0003^{(e)}$	$0.0003^{(e)}$–$0.06^{(j)}$	$0^{(f)}$	$0^{(f)}$–$0.33^{(f)}$
PRD	Crops. Meadows	$0.03^{(e)}$	$0.001^{(\epsilon)}$–$0.1^{(e)}$	$0.013^{(z)}$	$0.007^{(\iota)}$–$0.035^{(z)}$
PST	Grasslands	$0.09^{(\epsilon)}$	$0.001^{(\epsilon)}$–$0.15^{(\epsilon)}$	$0.171^{(\chi)}$	$0.013^{(z)}$–$0.66^{(\iota)}$
RMB	No Vegetation. Ravines	$0.0012^{(\Psi)}$	$0.0003^{(d)}$–$0.005^{(\omega)}$	$0.03^{(h,f)}$	$0^{(f)}$–$0.03^{(f)}$
SDN	No Vegetation. Bare Soil	$0.001^{(j)}$	$0.0002^{(\omega)}$–$0.04^{(k)}$	$0.03^{(h,f)}$	$0^{(f)}$–$0.22^{(f)}$
SNE	Artificial Coverage. Unbuilt Land	$0.0003^{(j)}$	$0.0002^{(\omega)}$–$0.04^{(a)}$	$0^{(f)}$	$0^{(f)}$–$0.22^{(f)}$
VAP	Artificial Coverage. Road, Parking or Unvegetated Pedestrian Areas	$0.03^{(e)}$	$0.0035^{(\Psi)}$–$0.5^{(e)}$	$1^{(y,\phi)}$	$0.02^{(\phi)}$–$2.5^{(\phi)}$
ZAU	Artificial Coverage. Artificial Green Area and Urban Trees	$0.4^{(d)}$	$0.03^{(j)}$–$1.3^{(x)}$	$3.5^{(y,\phi)}$	$3.5^{(z)}$–$14^{(z)}$
ZEV	Artificial Coverage. Extraction or Waste Areas	$0.1^{(e)}$	$0.0003^{(j)}$–$0.18^{(k)}$	$0.16^{(\omega,f)}$	$0^{(f)}$–$1^{(f)}$
ZQM	No Vegetation. Burnt Areas	$0.6^{(e)}$	$0.1^{(e)}$–$1.1^{(j)}$	$3.27^{(f)}$	$0.54^{(f)}$–$6^{(f)}$

trees; [72, 95] in vineyards; [26] in scrubs; and [96] in soils without vegetation and artificial coverages.

Also in Table 2.1, there are some values of z_0 and d arising from applications of specific numerical models with their land cover databases. For example, [75] used them in lakes and lagoons; [101] in rocky outcrops and rocks, evergreen forests, salt marshes, wetlands, bare soils, and artificial coverages; [21] in evergreen forests; [57] used in no citrus fruit trees; [82] in grasslands; and [81] in ravine and road, parking or unvegetated pedestrian areas.

Some papers dealing with collections of data from other authors, in particular from old publications, were useful too. In particular, the one by [4] used in estuaries, seas and oceans, and soils without vegetation; [23] in crops different from rice and artificial coverage; [89] in buildings, evergreen forests, glaciers and perpetual snow, scrubs, meadows, grasslands and artificial green area and urban trees; [28] in deciduous and evergreen forests; and [59] in crops different from rice, woody crops, meadows and grasslands. Also some early publications were used for constructing Table 2.1, such as [16], used in crops different from rice; [17] in glaciers and perpetual snow, meadows and grasslands; and [9, 43] in citrus fruit trees.

Finally, some of the current land cover databases based on remote sensing surveys (specifically, aircraft lidar and satellite images) that were taken into account are [24]: the NLCD database used in cliffs; [3]: the 1-km land cover data set DISCOVER (IGBP-DIS) for water courses; [6]: the CLC database applied in many coverages; and [98]: the LGN3 database used in rocky outcrops and rocks, salt marshes, soils without vegetation, and artificial coverages.

2.1.5 Roughness length and displacement height characterization

The SIOSE project uses a vectorial format, but, for convenience, we will translate it to a raster format. For this, we will define a grid with n_p points and, for each point, we will look for the mean value of basic coverages. Once we have the values of z_0 and d for each basic coverage, we can compute the specific z_0 and d values at any point using an appropriate weighted mean. This way, the SIOSE database will let us create a matrix with the percentage of the basic coverages at any point. This matrix is defined as follows: let M be an $n_p \times n_b$ matrix, with components $m_{i,j}$, where n_b is the number of basic coverages. For each row i of M, $m_{i,j}$ is the fraction of the basic coverage j at the point n_i ($m_{i,j} < 1$ and $\sum_{j=1}^{n_b} m_{i,j} = 1$).

When the ranges of z_0 and d are set for each basic land coverage, we can compute its values at any point of the terrain. Assuming that the values of z_0 and d are a certain mean of the values of the basic coverages z_{0j} and d_j, $j = 1, \ldots, n_b$, we can compute their values at any point. A simple weighted average may produce differences with the effective roughness of one order of magnitude. The study by [76] for the effective roughness length improves the formula proposed by [85], taking into account a non-dimensional patchiness parameter to consider the textural infor-

mation about the spatial dependence of the primitives (regions with specific properties) characterizing the surface inhomogeneity. However, generally the coverage information provided by the land cover databases (e.g., SIOSE) does not include the spatial distribution of basic coverages in a composed one, but only the fraction of the area covered by each surface type. So, in this case, only Taylor's formula was applied; in this approach, for a coverage i composed by n_b basic canopies with roughness length z_{0j}; $j = 1,\ldots,n_b$ on a fraction m_{ij} of the area, respectively, an approximation to the effective roughness length is given by computing the weighted geometric mean roughness length z_0:

$$z_0 = \prod_{j=1}^{n_b} z_{0j}^{m_{ij}}. \tag{2.1}$$

Regarding the displacement height, d, [76] and [85] did not study its estimation. In any case, the above mean formula is not appropriate for d, since, in the case of a basic coverage with displacement height equal to zero, it would produce a mean $z_0 = 0$ independently of the z_{0j} values of the other basic coverages. Some other works have studied the variation of d in several specific coverages, e.g., in urban [56] and vegetation [62, 100] canopies. One important conclusion is that the effective displacement height of a heterogeneous coverage can exceed the surface mean canopy height significantly. Taking this into account, we propose to use a weighted root mean square to obtain the highest mean value:

$$d = \sqrt{\sum_{j=1}^{n_b} m_{ij} d_j^2}, \tag{2.2}$$

where d_j and m_{ij} are the displacement height and the fraction of the basic coverage j in the composed one i, respectively. Figures 2.2(a) and (b) show the resulting composed z_0 and d values in Gran Canaria and La Palma Islands, considering the nominal values of the basic coverages given in Table 2.1. We remark that a weighted average version of that proposed by [69],

$$d = exp\left[\sum_{j=1}^{n_b} \frac{m_{ij}}{\ln d_j}\right]^{-1}, \tag{2.3}$$

which must be evaluated in the limit if any $d_j = 0$ or $d_j = 1$, is not appropriate in the case of any $d_j = 1$ since the average result of d would always be equal to 1, independently of the other d_j values. Similar conclusions may be reached from its application in the calculation of z_0 if any $z_{0j} = 1$. It can be noted that the application of this methodology to another database is straightforward.

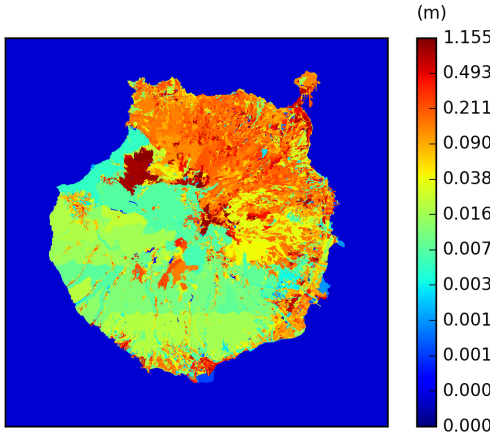

(a) Roughness length map of Gran Canaria

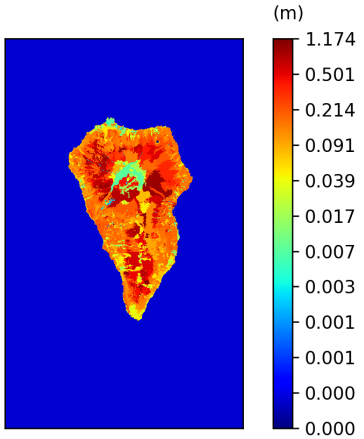

(b) Roughness length map of La Palma

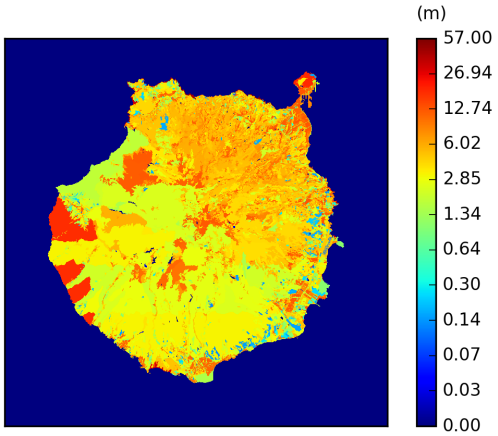

(c) Displacement height map of Gran Canaria

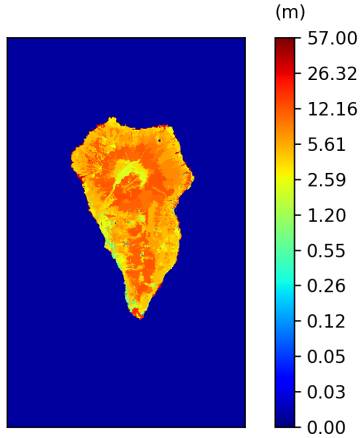

(d) Displacement height map of La Palma

Fig. 2.2: Roughness length and displacement height maps of Gran Canaria and La Palma islands (m) corresponding to the nominal values stated in Table 2.1 and using the mean values given in (2.1) and (2.2), respectively.

2.1.6 Literature review and characterization of albedo

The ranges of albedo ρ for each land cover have been obtained from a literature review. Table 2.2 summarizes it, and the specific references are listed in the caption. Here again, the first and second columns show the SIOSE code and a description for

each land coverages. The third and fourth columns present the nominal value and the range of ρ. Following the same procedure as for z_0 and d, we have taken the largest interval from those proposed by a wide list of authors.

Using the same nomenclature as in the roughness parameter characterization, we propose to compute the effective albedo at any point of a SIOSE polygon with an average of the mean values of the basic coverage albedo,

$$\rho = \sum_{j=1}^{n_b} m_{ij}\rho_j, \tag{2.4}$$

where ρ_j and m_{ij} are the albedo and the fraction of the basic coverage j in the composed one i, respectively.

Table 2.2: Albedo nominal values and ranges for SIOSE land cover classes. The superindex indicates the source:
(a) [2], (b) [50], (c) [80], (d) [66], (e) [33], (f) [94], (g) [19], (h) [49], (i) [27]

Code	Land Cover	ρ	ρ_{min}–ρ_{max}
ACM	Sea Cliffs	$0.2^{(a)}$	$0.05^{(b)}$–$0.7^{(b)}$
ACU	Water Courses	$0.14^{(c)}$	$0.03^{(d)}$–$1^{(d)}$
AEM	Water body. Reservoirs	$0.14^{(c)}$	$0.03^{(d)}$–$1^{(d)}$
AES	Estuaries	$0.1^{(a)}$	$0.03^{(d)}$–$1^{(d)}$
ALC	Coastal Lagoons	$0.1^{(a)}$	$0.03^{(d)}$–$1^{(d)}$
ALG	Water body. Lakes and Lagoons	$0.14^{(c)}$	$0.03^{(d)}$–$1^{(d)}$
AMO	Seas and Oceans	$0.1^{(a)}$	$0.03^{(d)}$–$1^{(e)}$
ARR	Rocky Outcrops and Rocks	$0.2^{(a)}$	$0.1^{(b)}$–$0.4^{(b)}$
CCH	Screes	$0.2^{(a)}$	$0.05^{(b)}$–$0.7^{(b)}$
CLC	Quaternary lava flow	$0.1^{(e)}$	$0.05^{(f)}$–$0.15^{(f)}$
CNF	Forest. Conifers	$0.14^{(e)}$	$0.05^{(d)}$–$0.15^{(d)}$
CHA	Herbaceous crops. Rice	$0.12^{(e)}$	$0.18^{(d)}$–$0.25^{(d)}$
CHL	Herbaceous crops. Different from Rice	$0.2^{(a)}$	$0.18^{(d)}$–$0.25^{(d)}$
EDF	Artificial Coverage. Buildings	$0.18^{(a)}$	$0.18^{(a)}$–$0.35^{(a)}$
FDC	Forest. Leafy. Deciduous	$0.16^{(a)}$	$0.10^{(e)}$–$0.5^{(a)}$
FDP	Forest. Leafy. Evergreen	$0.12^{(a)}$	$0.09^{(c)}$–$0.35^{(a)}$
GNP	No Vegetation. Glaciers and Perpetual Snow	$0.6^{(a)}$	$0.2^{(d)}$–$0.95^{(d)}$
HMA	Salt Marshes	$0.14^{(c)}$	$0.14^{(a)}$–$0.3^{(a)}$
HPA	Wetlands	$0.14^{(c)}$	$0.14^{(a)}$–$0.3^{(a)}$
HSA	Salt Mines	$0.5^{(g)}$	$0.166^{(e)}$–$0.5^{(g)}$
HSM	Salt Lakes	$0.5^{(g)}$	$0.166^{(e)}$–$0.5^{(g)}$
HTU	Peat bogs	$0.14^{(c)}$	$0.14^{(a)}$–$0.3^{(a)}$
LAA	Artificial Coverage. Artificial water body	$0.14^{(c)}$	$0.03^{(d)}$–$1^{(a)}$
LFC	Woody Crops. Citrus Fruit Trees	$0.18^{(a)}$	$0.13^{(h)}$–$0.22^{(h)}$
LFN	Woody Crops. No Citrus Fruit Trees	$0.18^{(a)}$	$0.13^{(h)}$–$0.22^{(h)}$
LOC	Other Woody Crops	$0.18^{(a)}$	$0.13^{(h)}$–$0.22^{(h)}$
LOL	Olive Groves	$0.18^{(a)}$	$0.13^{(h)}$–$0.22^{(h)}$

Table 2.2: *Continued*

Code	Land Cover	ρ	ρ_{min}–ρ_{max}
LVI	Vineyards	$0.18^{(a)}$	$0.14^{(a)}$–$0.5^{(a)}$
MTR	Scrubs	$0.25^{(a)}$	$0.14^{(c)}$–$0.5^{(a)}$
OCT	Artificial Coverage. Other Buildings	$0.16^{(a)}$	$0.16^{(a)}$–$0.45^{(a)}$
PDA	No Vegetation. Beaches, Dunes and Sandy Areas	$0.35^{(f)}$	$0.15^{(f)}$–$0.45^{(g)}$
PRD	Crops. Meadows	$0.2^{(a)}$	$0.1^{(e)}$–$0.6^{(a)}$
PST	Grasslands	$0.18^{(a)}$	$0.08^{(e)}$–$0.6^{(a)}$
RMB	No Vegetation. Ravines	$0.16^{(c)}$	$0.147^{(i)}$–$0.173^{(i)}$
SDN	No Vegetation. Bare Soil	$0.16^{(c)}$	$0.147^{(i)}$–$0.173^{(i)}$
SNE	Artificial Coverage. Unbuilt Land	$0.18^{(a)}$	$0.15^{(a)}$–$0.6^{(a)}$
VAP	Artificial Coverage. Road, Parking or Unvegetated Pedestrian Areas	$0.18^{(a)}$	$0.18^{(a)}$–$0.35^{(a)}$
ZAU	Artificial Coverage. Artificial Green Area and Urban Trees	$0.15^{(c)}$	$0.15^{(a)}$–$0.6^{(a)}$
ZEV	Artificial Coverage. Extraction or Waste Areas	$0.13^{(a)}$	$0.2^{(a)}$–$0.6^{(a)}$
ZQM	No Vegetation. Burnt Areas	$0.097^{(i)}$	$0.089^{(i)}$–$0.098^{(i)}$

2.2 Meteorological parameters

The wind is produced, firstly, as a consequence of spatial differences of barometric pressure, generally caused by the absorption of the solar radiation. In a horizontal plane, the wind flows from high pressure zones to low pressure ones, while vertically from low pressure zones to high pressure ones. Wind speed is proportional to the pressure variation per unity of length or pressure gradient. Zones of same pressures are represented in the weather maps joined by imaginary lines (isobars). The closer the isobars are to each other, the stronger the wind is.

A second factor that affects the air movement is the Coriolis force, caused by the Earth rotation. The term $f = 2\Theta\, sen\, \phi_l$ is called Coriolis parameter, where $\Theta = 7.292 \times 10^{-5}\ s^{-1}$ is the Earth rotation velocity and ϕ_l is the latitude. It is considered positive in the North Hemisphere, null in the Equator and negative in the South Hemisphere.

Thirdly, a centripetal acceleration may appear when the wind turns around a centre. Finally, also the friction because of the air movement must be considered. Winds affected by the pressure gradient and the Coriolis force are called geostrophic winds.

The Monin-Obukhov similarity theory leads to a division of the lowest layer of the atmosphere into several sublayers where the vertical wind profile is constructed in different ways. So, the planetary boundary layer is located at a height z_{pbl} over the terrain, and it is the layer under the free atmosphere that is directly affected by the friction of the Earth surface. In this case z_{pbl} is defined such that wind velocity is considered to be constant over it [77],

$$z_{pbl} = \frac{\gamma |\mathbf{v}^*|}{f} \tag{2.5}$$

where γ is a constant between 0.15 and 0.45 that depends on the atmospheric stability, and $\mathbf{v}^*$ is the friction velocity that is computed from wind measures or predictions.

The mixing layer, also called convective layer, is the atmospheric layer affected by convective phenomena caused by the surface heat. The air is well-mixed, that is, the wind and the potential temperature are almost constant with height. The height of the mixing layer h_m is approximated by:

$$h_m = \gamma' \sqrt{\frac{|\mathbf{v}^*| L}{f}} \tag{2.6}$$

where usually $\gamma' = 0.4$ [102] and L is the Monin-Obukhov length, that is computed with the Liu formulae [71],

$$\frac{1}{L} = a z_0^b \tag{2.7}$$

where a and b are defined by the Pasquill Stability Class(see Table 2.4).

The surface layer, located at a height z_{sl} over de terrain, is the lowest layer of the planetary boundary layer, just joining the terrain surface layer, where the drag friction force is dominant. The height of the surface layer is usually obtained [102],

$$z_{sl} = \frac{h_m}{10} \tag{2.8}$$

The atmospheric stability is related to the atmospheric turbulence as well as with the temperature gradient and the thermal inversion. It provides a qualitative measure of the air density variations because of pressure and temperature changes, and other phenomena that affect certain atmospheric movements.

The stability of the atmosphere may be classified as:

- **Stable atmosphere.** If a mass of air goes up, it will be surrounded by hotter air and thus, less dense than it. This will make go down. If It goes down, It will be surrounded by colder air (denser) and will tend to go up. This air trend of staying in the same layer is called stability of the atmospheric stratification.
- **Unstable atmosphere.** Under unstable conditions, the potential temperature decreases with height, increasing the vertical movements, that is, if the air goes up, it will be surrounded by colder and denser air and it will tend to continue going up; and if it goes down, it will find hotter and lighter air, and it will tend to continue going down.
- **Neutral atmosphere.** If a mass of air (after a vertical movement in an atmospheric layer without mixing with the surrounding air) experiments a null vertical net force, the ascending movements will not be affected by the thermal gradient and the atmosphere layer is assumed to be neutrally stratified. Under such

conditions, this mass of air does not tend to regret to it original position (stable atmosphere) nor accelerates going away from it (unstable stratification).

The atmospheric stability was usually characterized by the Table 2.3 including the Pasquill stability classes.

Table 2.3: Pasquill stability classes depending on surface wind speeds and isolation. Strong isolation corresponds to the typical sunny noon of the middle summer in England; light isolation, to similar conditions in middle winter. Night is referred to the period between one hour before sunset and one hour after sunrise. Neutral class D should also be used for overcast skies during the day or the night, and for any sky condition during the preceding and following night hours defined above.

Pasquill stability class					
	Isolation			**Night**	
Surface wind speed (m/s)	**Strong**	**Moderate**	**Light**	**Overcast $\geq 4/8$ clouds**	**$\leq 3/8$ clouds**
< 2	A	A-B	B	-	-
$2-3$	A-B	B	C	E	F
$3-5$	B	B-C	C	D	E
$5-6$	C	C-D	D	D	D
> 6	C	D	D	D	D
For A-B, take the average of A and B values, etc.					

Table 2.4: Values of the parameters a and b to calculate Monin-Obukhov length depending on the Pasquill stability class.

Pasquill stability class	**a**	**b**
A (Extremely unstable)	-0.08750	-0.1029
B (Moderately unstable)	-0.03849	-0.1714
C (Lightly unstable)	-0.00807	-0.3049
D (Neutral)	0.00000	0.0000
E (Lightly stable)	0.00807	-0.3049
F (Moderately stable)	0.03849	-0.1714

Usually, the anemometers provide measures of turbulence intensity that may help to complete the information about the type of atmospheric stability of the region. The turbulence intensity i is defined as the squared root of the sum of the variances, $\sigma_u^2, \sigma_v^2, \sigma_w^2$, of the three components of the wind velocity u_0, v_0, w_0, respectively, divided by the average of the measure wind speeds,

$$i = \frac{\sqrt{\sigma_u^2 + \sigma_v^2 + \sigma_w^2}}{|\mathbf{v}_0|} \tag{2.9}$$

In practice, we only have measures of intensity variations of the speed but not of the direction. In such cases, equation (2.9) yields:

$$i = \frac{\sigma_{v_0}}{|\mathbf{v}_0|} \tag{2.10}$$

where σ_{v_0} represents the standard deviation of the measured wind intensities.

An unstable atmosphere means a high level of turbulence, with a range of turbulence intensities between 0.2 and 0.4, approximately. However, a stable atmosphere, with a small turbulence or an almost null one, is characterized by intensities between 0.05 and 0.01. Table 2.5 illustrate the relation of the turbulence intensity and the atmospheric stability.

Table 2.5: Pasquill stability classes depending on the surface wind speed and the turbulence intensity.

	Pasquill stability class						
Surface wind	**Isolation**				**Night**		
speed (m/s)	$i > 0.35$	$0.35 \geq i > 0.25$	$0.25 \geq i > 0.15$	$0.15 \geq i$	$i > 0.075$	$0.075 \geq i > 0.03$	$0.03 \geq i$
$\lvert v_0 \rvert < 2$	A	B	B	B	F	F	F
$2 \leq \lvert v_0 \rvert < 3$	A	B	C	C	E	E	F
$3 \leq \lvert v_0 \rvert < 5$	B	B	C	C	D	E	E
$\lvert v_0 \rvert \geq 5$	C	C	C	D	D	D	D

The concepts of Neutral and Stable Boundary Layers (SBL) have been revised to consider the effect of the free-flow static stability and baroclinicity on the turbulent transport of momentum and scalars in the boundary layer, as well as the model of turbulent entrainment for Convective Boundary Layers (CBL) [104]. Accordingly, different types of SBL regimes can be distinguished: truly neutral (absence of any buoyancy effects throughout the PBL); conditionally neutral (buoyancy flux at the surface is negligible); short-lived nocturnal (separated from the free atmosphere by near-neutral residual layers); and long-lived (immediately adjoining the stably stratified free atmosphere). The SBL height, h, may be evaluated according to the expression recently introduced by [103]. This expression represents a multi-limit equation for the equilibrium PBL height that covers the types mentioned earlier of neutral and stable conditions in the atmosphere. In contrast to the stable and neutral cases, the estimation of the CBL height is not straightforward, since our model is diagnostic and the recommended parameterizations are prognostic. To overcome this problem, some prognostic data must be used. In this approach, the CBL height is obtained from the results of the mesoscale model, e.g., HARMONIE-AROME model.

The estimation of the PBL height is calculated separately for stable/neutral conditions and convective conditions. For this, the Brunt-Väisälä frequency N in the PBL and the surface buoyancy flux B_s allow to characterize atmospheric stability:

$$N^2 = \frac{g}{T}\left(\frac{\partial T}{\partial z} + \Gamma_d\right), \tag{2.11}$$

g being the gravity acceleration, T a reference value of the air absolute temperature, z the height variable and $\Gamma_d = 9.8 \times 10^{-3}$ K/m the dry adiabatic lapse rate If $N^2 \geq 0$, the atmosphere is considered stable/neutral. However, $N^2 < 0$ indicates a CBL.

In stable/neutral atmosphere (SBL), the formula to compute the SBL height was proposed by [103]:

$$h = \gamma u_* / f, \tag{2.12}$$

where u_* is the surface friction velocity, f the Coriolis parameter defined as $f = 2\omega \sin\phi$ (ω is the Earth rotation and ϕ the latitude), and γ is a function of the imposed-stability parameter $\mu_N = N_{2h-h}/f$ in the free atmosphere:

$$\gamma = \gamma_0 \left(1 + \frac{\gamma_0^2 C_{uN}}{C_s^2}\mu_N\right)^{-1/2}, \tag{2.13}$$

Experimental data suggest $\gamma_0 = 0.5$, $C_{uN}/C_s^2 = 0.6$; N_{2h-h} is the free-flow Brunt-Väisälä frequency in the free atmosphere immediately above the SBL ($h < z < 2h$). In particular, the stable/neutral PBL may be classified as: truly neutral (TN) at $\mu_N = 0$ (B_s and $N_{2h-h} = 0$); conditionally neutral (CN) usually at $0.5 \times 10^2 < \mu_N < 3 \times 10^2$ ($B_s \geq 0$ and $N_{2h-h} > 0$); nocturnal stable (NS) at ($B_s < 0$ and $N_{2h-h} = 0$); and long-lived stable (LS) at ($B_s < 0$ and $N_{2h-h} > 0$).

2.3 Conclusions

Some essential data and parameter definitions for wind and solar radiation modeling have been introduced in this chapter. From the geographical point of view, one must have information about the orography of the surface involved in the simulation and the land cover distribution of such surface. On the one hand, nowadays, DEM allows to construct meshes adapted to a terrain surface to be used in the discretization of a problem. On the other hand, the study of the roughness parameters associated to an accurate knowledge of the land coverages provides a valuable tool for a better wind field description. In the same way, the setting up of each land coverage albedo is important to obtain reliable values of reflection in solar radiation modeling.

References

1. Acreman, M.C., Harding, R.J., Lloyd, C.R., McNeil, D.D.: Evaporation characteristics of wetlands: experience from a wet grassland and a reedbed using eddy correlation measurements. Hydrology and Earth System Sciences **7**(1), 11–21 (2003). DOI 10.5194/hess-7-11-2003

2. Adrian, G., Fiedler, F.: Simulation of unstationary wind and temperature fields over complex terrain and comparison with observations. Beitr Phys Atmosph **64**, 27–48 (1991)
3. Belward, A.S., Estes, J.E., Kline, K.D.: The IGBP-DIS global 1-km land-cover data set DIS-Cover: A project overview. Photogramm Eng Rem S **65**(9), 1013–1020 (1999)
4. Blocken, B., van der Hout, A., Dekker, J., Weiler, O.: CFD simulation of wind flow over natural complex terrain: Case study with validation by field measurements for Ria de Ferrol, Galicia, Spain. J Wind Eng Ind Aerod **147**, 43–57 (2015)
5. Blumberg, D.G., Greeley, R.: Field studies of aerodynamic roughness length. J Arid Environ **25**, 39–48 (1993)
6. Bossard, M., Feranec, J., Otahel, J.: CORINE land cover technical guide – Addendum 2000. Tech. rep., European Environment Agency, Copenhagen (2000)
7. Bosveld, F.C.: Derivation of fluxes from profiles over a moderately homogeneous forest. Bound-Lay Meteorol **84**(2), 289–327 (1997). DOI 10.1023/a:1000453629876. URL http://dx.doi.org/10.1023/a:1000453629876
8. Bottema, M., Mestayer, P.G.: Urban roughness mapping – validation techniques and some first results. J Wind Eng Ind Aerod **74-76**, 163–173 (1998). DOI 10.1016/s0167-6105(98)00014-2. URL http://dx.doi.org/10.1016/s0167-6105(98)00014-2
9. Brooks, F.A.: An Introduction to Physical Micrometeorology. University of California, Davis, California (1959)
10. Brutsaert, W.: Evaporation into the atmosphere. D. Reidel Publish Company, Dordrecht, Holland (1982)
11. Campbell, D.R., Lavoie, C., Rochefort, L.: Wind erosion and surface stability in abandoned milled peatlands. Can J Soil Sci **82**(1), 85–95 (2002). DOI 10.4141/s00-089. URL http://dx.doi.org/10.4141/s00-089
12. Chang, Y., Tan, J., Grimmond, S., Tang, Y.: Distribution of Aerodynamic Roughness Based on Land Cover and DEM-A Case Study in Shanghai, China. In: ICUC9 - 9th International Conference on Urban Climate jointly with 12th Symposium on the Urban Environment (2015)
13. Claassen, H.C., Riggs, A.C.: An estimate of the roughness length and displacement height of Sonoran Desert vegetation, South-Central Arizona. U.S. Geological Survey. Tech. rep., Water-Resources Investigations Report 92-4065, Denver, Colorado (1993)
14. Coceal, O., Belcher, S.E.: A canopy model of mean winds through urban areas. Q J Roy Meteorol Soc **130**(599), 1349–1372 (2004). DOI 10.1256/qj.03.40. URL http://dx.doi.org/10.1256/qj.03.40
15. Colin, J., Faivre, R.: Aerodynamic roughness length estimation from very high-resolution imaging lidar observations over the heihe basin in china. Hydrol. Earth Syst. Sci. **14**, 2661–2669 (2010). DOI 10.5194/hess-14-2661-2010
16. Davenport, A.G.: The dependence of wind loads on meteorological parameters. In: Conference on Wind Loads on Buildings. University of Toronto Press, Toronto (1967). Paper 2
17. Deacon, E.L.: Vertical Profiles of Mean Wind in the Surface Layers of the Atmosphere, Meteorol Off Geoph Mem 91. Tech. rep., Meteorological Office, United Kingdom (1953)
18. DeBruin, H.A.R., Moore, C.J.: Zero-plane displacement and roughness length for tall vegetation, derived from a simple mass conservation hypothesis. Bound-Lay Meteorol **31**(1), 39–49 (1985)
19. Dobos, E.: Albedo. Encyclopedia of soil science **2**, 24–25 (2006)
20. Dong, Z., Gao, S., Fryrear, D.W.: Drag coefficients, roughness length and zero-plane displacement height as disturbed by artificial standing vegetation. J Arid Environ **49**(3), 485–505 (2001). DOI 10.1006/jare.2001.0807. URL http://dx.doi.org/10.1006/jare.2001.0807
21. Dorman, J.L., Sellers, P.J.A.: Global climatology of albedo, roughness length and stomatal resistance for atmospheric general circulation models as represented by the simple biosphere model (SiB). J Appl Meteorol **28**(9), 833–855 (1989)
22. Drennan, W.M., Taylor, P.K., Yelland, M.J.: Parameterizing the sea surface roughness. J. Phys. Oceanogr. **35**(5), 835–848 (2005). DOI 10.1175/jpo2704.1. URL http://dx.doi.org/10.1175/jpo2704.1

23. ESDU: Characteristics of wind speed in the lower layers of the atmosphere near the ground: Strong winds (neutral atmosphere). Tech. rep., Engineering Sciences Data Unit, Regent Street, London, UK (1972)
24. Fry, J.A., Xian, G., Jin, S., Dewitz, J.A., Homer, C.G., Yang, L., Barnes, C.A., Herold, N.D., Wickham, J.D.: Completion of the 2006 National Land Cover Database for the Conterminous United States. Photogramm Eng Rem S **77**(9), 858–864 (2011)
25. Gao, Z., Wang, L., Bi, X., Song, Q., Gao, Y.: A simple extension of "an alternative approach to sea surface aerodynamic roughness" by Zhiqiu Gao, Qing Wang, and Shouping Wang. J Geophys Res **117**(D16110), 1–8 (2012). DOI 10.1029/2012jd017478. URL http://dx.doi.org/10.1029/2012jd017478
26. Garratt, J.R.: Surface influence upon vertical profiles in the atmospheric near-surface layer. Q J Roy Meteorol Soc **106**(450), 803–819 (1980). DOI 10.1002/qj.49710645011. PB
27. Giambelluca, T.W., Hölscher, D., Bastos, T.X., Frazão, R.R., Nullet, M.A., Ziegler, A.D.: Observations of albedo and radiation balance over postforest land surfaces in the eastern amazon basin. Journal of Climate **10**(5), 919–928 (1997)
28. Graefe, J.: Roughness layer corrections with emphasis on SVAT model applications. Agr Forest Meteorol **124**(3–4), 237–251 (2004). DOI 10.1016/j.agrformet.2004.01.003
29. Graf, A., van de Boer, A., Moene, A., Vereecken, H.: Intercomparison of methods for the simultaneous estimation of zero-plane displacement and aerodynamic roughness length from single-level eddy-covariance data. Bound-Lay Meteorol **151**(2), 373–387 (2014). DOI 10.1007/s10546-013-9905-z. URL http://dx.doi.org/10.1007/s10546-013-9905-z
30. Grimmond, C.S.B., Oke, T.R.: Aerodynamic properties of urban areas derived from analysis of surface form. J Appl Meteorol **38**(9), 1262–1292 (1999)
31. Hammond, D.S., Chapman, L., Thornes, J.E.: Roughness length estimation along road transects using airborne LIDAR data. Meteorol Appl **19**(4), 420–426 (2012). DOI 10.1002/met.273. URL http://dx.doi.org/10.1002/met.273
32. Hanna, S.R., Chang, J.C.: Boundary layer parameterizations for applied dispersion modeling over urban areas. Bound-Lay Meteorol **58**(3), 229–259 (1992). DOI 10.1007/BF02033826
33. Hansen, F.V.: Albedos. Tech. Rep. ARL-TR-57, U.S. Army Research Laboratory, AMSRL-BE, White Sands Missile Range, NM 88002-5501 (1993)
34. Hansen, F.V.: Surface roughness lengths. Tech. Rep. ARL-TR-61, U.S. Army Research Laboratory, AMSRL-BE, White Sands Missile Range, NM 88002-5501 (1993)
35. Hazeu, G.W., Schuiling, C., Dorland, G.J., Roerink, G.J., Naeff, H.S.D., Smidt, R.A.: Landelijk Grondgebruiksbestand Nederland versie 7 (LGN7). vervaardiging, nauwkeurigheid en gebruik. Tech. rep., Alterra Wageningen UR, Wageningen (2014). In Dutch
36. Hicks, B.B., Hyson, P., Moore, C.J.: A study of eddy fluxed over a forest. J Appl Meteorol **14**(1), 58–66 (1975)
37. Holland, D.E., Berglund, J.A., Spruce, J.P., McKellip, R.D.: Derivation of effective aerodynamic surface roughness in urban areas from airborne lidar terrain data. J Appl Meteorol and Clim **47**(10), 2614–2626 (2008). DOI 10.1175/2008JAMC1751.1
38. Holt, T., Pullen, J.: Urban canopy modeling of the New York City Metropolitan Area: A comparison and validation of single- and multilayer parameterizations. Mon Weather Rev **135**(5), 1906–1930 (2007). DOI 10.1175/mwr3372.1. URL http://dx.doi.org/10.1175/mwr3372.1
39. Hsu, S.A.: A Dynamic Roughness Equation and Its Application to Wind Stress Determination at the Air-Sea Interface. J Phys Oceanogr **4**(1), 116–120 (1974). DOI 10.1175/1520-0485(1974)004¡0116:ADREAI¿2.0.CO;2. URL http://dx.doi.org/10.1175/1520-0485(1974)004¡0116:ADREAI¿2.0.CO;2
40. van den Hurk, B.J.J.M.: Sparse canopy parameterization for meteorological models. Ph.D. thesis, Dept. of Meteorology, WAU, Wageningen, The Netherlands (1995)
41. Hurtalová, T., Matejka, F.: Surface characteristics and energy fluxes above different plant canopies. Agr Forest Meteorol **98-99**, 491–500 (1999). DOI 10.1016/S0168-1923(99)00118-5
42. Jacobs, A.F.G., Boxel, J.H.: Changes of the zero-plane displacement and aerodynamic roughness length of maize during the growing season. Agr Forest Meteorol **42**, 53–62 (1988). DOI 10.1016/0168-1923(88)90066-4

43. Kalma, J.D., Fuchs, M.: Citrus orchards. In: J.L. Monteith (ed.) Vegetation and the Atmosphere. Academic Press, London (1976)
44. Kanda, M., Kanega, M., Kawai, T., Moriwaki, R., Sugawara, H.: Roughness lengths for momentum and heat derived from outdoor urban scale models. J Appl Meteorol Clim **46**(7), 1067–1079 (2007). DOI 10.1175/jam2500.1. URL http://dx.doi.org/10.1175/jam2500.1
45. Kanda, M., Moriwaki, R., Roth, M., Oke, T.: Area-averaged sensible heat flux and a new method to determine zero-plane displacement length over an urban surface using scintillometry. Bound-Lay Meteorol **105**(1), 177–193 (2002). DOI 10.1023/a:1019668424982. URL http://dx.doi.org/10.1023/a:1019668424982
46. Kimura, R., Kondo, J.: Heat balance model over a vegetated area and its application to a paddy field. J Meteorol Soc Jpn Ser II **76**(6), 937–953 (1998)
47. Kondo, J., Yamazawa, H.: Aerodynamic roughness over an inhomogeneous ground surface. Bound-Lay Meteorol **35**(4), 331–348 (1986). DOI 10.1007/bf00118563. URL http://dx.doi.org/10.1007/bf00118563
48. Kustas, W.P., Choudhury, B.J., Kunkel, K.E., Gay, L.W.: Estimate of the aerodynamic roughness parameters over an incomplete canopy cover of cotton. Agr Forest Meteorol **46**(1-2), 91–105 (1989). DOI 10.1016/0168-1923(89)90114-7. URL http://dx.doi.org/10.1016/0168-1923(89)90114-7
49. Landsberg, J., Powell, D., Butler, D.: Microclimate in an apple orchard. Journal of Applied Ecology pp. 881–896 (1973)
50. Larson, D.W., Matthes, U., Kelly, P.E.: Cliff ecology: pattern and process in cliff ecosystems. Cambridge University Press (2005)
51. Lettau, H.H.: Note on the aerodynamic roughness-parameter estimation on the basis of roughness-element description. J Appl Meteorol **8**(5), 828–832 (1969)
52. Li, X., Feng, G., Sharratt, B., Zheng, Z.: Aerodynamic properties of agricultural and natural surfaces in northwestern Tarim Basin. Agr Forest Meteorol **204**, 37–45 (2015). DOI 10.1016/j.agrformet.2015.01.005. URL http://dx.doi.org/10.1016/j.agrformet.2015.01.005
53. MacArthur, C.D., Haines, P.A.: The roughness lengths associated with regions of heterogeneous vegetation and elevation. Tech. Rep. Contract DAAD7-8-D-0206, University of Dayton Research Institute, Dayton, OH 45469 (1982)
54. Mahrt, L., Vickers, D., Edson, J., Wilczak, J.M., Hare, J., Højstrup, J.: Vertical structure of turbulence in offshore flow during rasex. Bound-Lay Meteorol **100**(1), 47–61 (2001)
55. Medeiros, S.C., Hagen, S.C., Weishampel, J.F.: Comparison of floodplain surface roughness parameters derived from land cover data and field measurements. J Hydrol **452-453**, 139–149 (2012). DOI 10.1016/j.jhydrol.2012.05.043. URL http://dx.doi.org/10.1016/j.jhydrol.2012.05.043
56. Millward-Hopkins, J.T., Tomlin, A.S., Ma, L., Ingham, D., Pourkashanian, M.: Estimating aerodynamic parameters of urban–like surfaces with heterogeneous building heights. Bound-Lay Meteorol **141**(3), 443–465 (2011). DOI 10.1007/s10546-011-9640-2. URL http://dx.doi.org/10.1007/s10546-011-9640-2
57. Mochida, A., Murakami, S., Toshio-Ojima, Kim, S., Ooka, R., Sugiyama, H.: CFD analysis of mesoscale climate in the greater tokyo area. J Wind Eng Ind Aerod **67-68**, 459–477 (1997). DOI 10.1016/s0167-6105(97)00060-3. URL http://dx.doi.org/10.1016/s0167-6105(97)00060-3
58. Molero-Paredes, T., Matos, A.: Efectos de la inducción artificial de la poliploidia en plantas de aloe vera(l.). Boletín del Centro de Investigaciones Biológicas **42**(1), 111–133 (2008). In Spanish
59. Monteith, J.L., Unsworth, M.H.: Principles of Environmental Physics. Edward Arnold, LTD, New York, 291 pp. (1990)
60. Montero, G., Rodríguez, E., Oliver, A., Calvo, J., Escobar, J.M., Montenegro, R.: Optimisation technique for improving wind downscaling results by estimating roughness parameters. J Wind Eng Ind Aerod (2018). In press
61. Moore, P.A., Pypker, T.G., Waddington, J.M.: Effect of long-term water table manipulation on peatland evapotranspiration. Agricultural and Forest Meteorology **178–179**, 106–119 (2013). DOI 10.1016/j.agrformet.2013.04.013

62. Nakai, T., Sumida, A., Daikoku, K., Matsumoto, K., van der Molen, M.K., Kodama, Y., Kononov, A.V., Maximov, T.C., Dolman, A.J., Yabuki, H., Hara, T., Ohta, T.: Parameterisation of aerodynamic roughness over boreal, cool- and warm-temperate forests. Agr Forest Meteorol **148**(12), 1916–1925 (2008). DOI 10.1016/j.agrformet.2008.03.009. URL http://dx.doi.org/10.1016/j.agrformet.2008.03.009
63. Nakai, T., Sumida, A., Matsumoto, K., Daikoku, K., Iida, S., Park, H., Miyahara, M., Kodama, Y., Kononov, A.V., Maximov, T.C., Yabuki, H., Hara, T., Ohta, T.: Aerodynamic scaling for estimating the mean height of dense canopies. Bound-Lay Meteorol **128**(3), 423–443 (2008). DOI 10.1007/s10546-008-9299-5. URL http://dx.doi.org/10.1007/s10546-008-9299-5
64. National Technique Team SIOSE: Documento Técnico SIOSE2005 – Versión 2.2. Tech. rep., D.G. Instituto Geográfico Nacional, Madrid (2011). In Spanish
65. National Technique Team SIOSE: Manual de Fotointerpretación SIOSE - Versión 2. Tech. rep., D.G. Instituto Geográfico Nacional, Madrid (2011). In Spanish
66. Oke, T.R.: Boundary layer climates. Routledge (2002)
67. Parlange, M.B., Brutsaert, W.: Regional roughness of the landes forest and surface shear stress under neutral conditions. Bound-Lay Meteorol **48**(1-2), 69–81 (1989). DOI 10.1007/BF00121783
68. Pires, L.B.M., Fisch, G., Gielow, R., Souza, L.F., Avelar, A.C., De-Paula, I.B., Girardi, R.D.M.: A study of the internal boundary layer generated at the alcantara space center. Am J Environ Eng **5**(1A), 82–64 (2015). DOI 10.5923/s.ajee.201501.08. URL http://dx.doi.org/10.5923/s.ajee.201501.08
69. Qualls, R.J., Brutsaert, W.: Effect of vegetation density on the parameterization of scalar roughness to estimate spatially distributed sensible heat fluxes. Water Resour. Res. **32**(3), 645–652 (1996)
70. Randall, J.M.: Wind profiles in an orchard plantation. Agr Forest Meteorol **6**(6), 439–452 (1969)
71. Ratto, C.: The aiolos and wlnds codes. In: Modelling of Atmospheric Flow Fields, pp. 421–431. World Scientific (1996)
72. Riou, C., Pieri, P., Valancogne, C.: Variation de la vitesse du vent à l'intérieur et au-dessus d'une vigne. Agr Forest Meteorol **39**, 143–154 (1987). In French
73. Roballo, S.T., Fisch, G.: Escoamento atmosfétrico no Centro de Lançamento de Alcântara (CLA): Parte I - Aspectos observcionais. Rev Bras Meteorol **23**(4), 510–519 (2008). DOI 10.1590/S0102-77862008000400010. In Portuguese
74. Rotach, M.W.: Determination of the zero plane displacement in an urban environment. Bound-Lay Meteorol **67**(1–2), 187–193 (1994). DOI 10.1007/BF00705513
75. Sacré, C., Moisselin, J.M., Sabre, M., Flori, J.P., Dubuisson, B.: A new statistical approach to extreme wind speeds in france. J Wind Eng Ind Aerod **95**(9-11), 1415–1423 (2007). DOI 10.1016/j.jweia.2007.02.013
76. Schmid, H.P., Bunzli, B.: The influence of surface texture on the effective roughness length. Q J Roy Meteorol Soc **121**(521), 1–21 (1995). DOI 10.1002/qj.49712152102
77. Sempreviva, A.: Roughness changes: response of neutral boundary layers. In: Modelling of Atmospheric Flow Fields, pp. 213–245. World Scientific (1996)
78. Shimoyama, K., Hiyama, T., Fukushima, Y., Inoue, G.: Controls on evapotranspiration in a west siberian bog. Journal of Geophysical Research: Atmospheres **109**(D8), 1–12 (2004). DOI 10.1029/2003JD004114
79. Stanhill, G.: A simple instrument for the field measurement of a turbulent diffusion flux. J Appl Meteorol **8**(4), 509–513 (1969)
80. Steyaert, L.T., Knox, R.G.: Reconstructed historical land cover and biophysical parameters for studies of land-atmosphere interactions within the eastern united states. Journal of Geophysical Research: Atmospheres **113**(D2) (2008)
81. Su, Z.: An introduction to the surface energy balance system (SEBS). Lecture notes, ESA TIGER Capacity Building Facility 1st Training Course on Advanced optical remote sensing (2006)

82. Su, Z., Schmugge, T., Kustas, W.P., Massman, W.J.: An evaluation of two models for estimation of the roughness height for heat transfer between the land surface and the atmosphere. J Appl Meteorol **40**(11), 1933–1951 (2001)
83. Takagi, K., Miyata, A., Harazono, Y., Ota, N., Komine, M., Yoshimoto, M.: An alternative approach to determining zero-plane displacement, and its application to a lotus paddy field. Agr Forest Meteorol **115**, 173–181 (2003)
84. Tanaka, S., Sugawara, H., Narita, K., Yokoyama, H., Misaka, I., Matsushima, D.: Zero-Plane Displacement Height in a Highly Built-Up Area of Tokyo. SOLA **7**, 93–96 (2011). DOI 10.2151/sola.2011-024. URL http://dx.doi.org/10.2151/sola.2011-024
85. Taylor, P.A.: Comments and further analysis on effective roughness lengths for use in numerical three-dimensional models. Bound-Lay Meteorol **39**, 403–418 (1987)
86. Thom, A.S.: Momentum absorption by vegetation. Q J Roy Meteorol Soc **97**(414), 414–428 (1971)
87. Thom, A.S.: Momentum, mass and heat exchange of vegetation. Q J Roy Meteorol Soc **98**(415), 124–134 (1972)
88. Tian, X., Li, Z.Y., van der Tol, C., Su, Z., Li, X., He, Q.S., Bao, Y.F., Chen, E.X., Li, L.H.: Estimating zero-plane displacement height and aerodynamic roughness length using synthesis of lidar and spot-5 data. Remote Sensing of Environment **115**(9), 2330–2341 (2011). DOI 10.1016/j.rse.2011.04.033
89. Tieleman, H.W.: Roughness estimation for wind-load simulation experiments. J Wind Eng Ind Aerod **91**(9), 1163–1173 (2003). DOI 10.1016/S0167-6105(03)00058-8
90. Troen, I., Petersen, E.L.: European Wind Atlas, 300 pp. Tech. rep., Risø National Laboratory, Roskilde, Denmark (1989)
91. van Wijk, B.M.: Predicting the rooftop wind climate for urban wind energy in the Rotterdam - Delft - Zoetermeer region. new approaches for implementing urban height data in the wind atlas method. Tech. rep., Eindhoven University of Technology, Eindhoven (2011). 114 pp.
92. Verhoef, A., McNaughton, K.G., Jacobs, A.F.G.: A parameterization of momentum roughness length and displacement height for a wide range of canopy densities. Hydrol Earth Syst Sci **1**(1), 81–91 (1997). DOI 10.5194/hess-1-81-1997. URL http://dx.doi.org/10.5194/hess-1-81-1997
93. Villalobos, F.J., Orgaz, F., Testi, L., Fereres, E.: Measurement and modeling of evapotranspiration of olive (Olea europaea L.) orchards. Eur J Agron **13**(2-3), 155–163 (2000). DOI 10.1016/s1161-0301(00)00071-x. URL http://dx.doi.org/10.1016/s1161-0301(00)00071-x
94. Warner, T.T.: Desert meteorology. Cambridge University Press (2009)
95. Weiss, A., Allen, L.H.: Vertical and horizontal air flow above rows of a vineyard. Agr Meteorol **17**(6), 433–452 (1976). DOI 10.1016/0002-1571(76)90021-2
96. Wieringa, J.: Updating the Davenport roughness classification. J Wind Eng Ind Aerod **41**(1-3), 357–368 (1992). DOI 10.1016/0167-6105(92)90434-C
97. WindSim AS: Wind Resource Assessment – Annual Energy Production. Project: Hundhammer_WS_Express. Tech. rep., WindSim AS, Fjordgaten 15, N- 3125 Tønsberg, Norway (2014). 29 pp.
98. de Wit, A.J.W., Van der Heijden, T.G.C., Thunnissen, H.A.M.: Vervaardiging en nauwkeurigheid van het LGN3-grondgebruiksbestand. Tech. rep., DLO-Staring Centrum, Wageningen (1999). In Dutch
99. Yang, K., Koike, T., Ishikawa, H., Kim, J., Li, X., Liu, H., Liu, S., Ma, Y., Wang, J.: Turbulent flux transfer over bare-soil surfaces: Characteristics and parameterization. J Appl Meteorol Clim **47**(1), 276–290 (2008). DOI 10.1175/2007jamc1547.1. URL http://dx.doi.org/10.1175/2007jamc1547.1
100. Yang, R., Friedl, M.A.: Determination of roughness lengths for heat and momentum over boreal forests. Bound-Lay Meteorol **107**(3), 581–603 (2003). DOI 10.1023/a:1022880530523. URL http://dx.doi.org/10.1023/a:1022880530523
101. Yoon, J.J., Shim, J.S., Park, K.S., Lee, J.C.: Numerical experiments of storm winds, surges, and waves on the southern coast of Korea during Typhoon Sanba: the role of revising wind force. Nat Hazards Earth Sys Sci **14**(12), 3279–3295 (2014). DOI 10.5194/nhess-14-3279-2014

102. Zannetti, P.: Air pollution modeling. Comp. Mech. Publications, Southampton (UK) (1990)
103. Zilitinkevich, S.S., Esau, I.N.: On integral measures of the neutral barotropic planetary boundary layer. Bound-Lay Meteorol **104**, 371–379 (2002)
104. Zilitinkevich, S.S., Tyuryakov, S.A., Troitskaya, Y.I., Mareev, E.A.: Theoretical models of the height of the atmospheric boundary layer and turbulent entrainment at its upper boundary. Atmospheric and Oceanic Physics **48**(1), 150–160 (2012). DOI 10.1134/S0001433812010148